Research Article Vol. 32, No. 14 / 1 Jul 2024 / Optics Express 24615
Optics EXPRESS

High speed single pixel imaging using a microLED-on-CMOS light projector

G. E. Johnstone,[1,*] J. Gray,[1] S. Bennett,[2] S. D. Johnson,[3] C. F. Higham,[4] F. Dehkhoda,[5] E. Xie,[1] J. Herrnsdorf,[1] P. Murray,[2] M. J. Padgett,[3] R. Murray-Smith,[4] R. K. Henderson,[5] M. D. Dawson,[1] and M. J. Strain[1]

[1]*Institute of Photonics, Department of Physics, University of Strathclyde, Technology and Information Centre, 99 George Street, G1 1RD, Glasgow, United Kingdom*
[2]*Department of Electronic and Electrical Engineering, University of Strathclyde, Royal College Building, 204 George Street, G1 1XW, Glasgow, United Kingdom*
[3]*School of Physics and Astronomy, University of Glasgow, G12 8QQ, Glasgow, United Kingdom*
[4]*School of Computing Science, University of Glasgow, Glasgow G12 8QQ, United Kingdom*
[5]*School of Engineering, University of Edinburgh, Sanderson Building, Robert Stevenson Road, EH9 3FB, Edinburgh, United Kingdom*
[*]*g.johnstone@strath.ac.uk*

Abstract: Achieving high frame-rate operation in single pixel imaging schemes normally demands significant compromises in the flexibility of the imaging system, requiring either complex optical setups or a hardware-limited pattern mask set. Here, we demonstrate a single pixel imaging capability with pattern frame-rates approaching 400 kfps with a recently developed microLED light projector and an otherwise simple optical setup. The microLED array has individually addressable pixels and can operate significantly faster than digital micromirror devices, allowing flexibility with regards to the pattern masks employed for imaging even at the fastest frame-rates. Using a full set of Hadamard or Noiselet patterns, we demonstrate 128×128 pixel images being generated at 7.3 fps. We generate a pattern set specifically for the light projector using deep learning tools and use these patterns to demonstrate single pixel imaging at almost 800 fps.

1. Introduction

Single pixel imaging, where 2D images can be captured using a spatial light modulation element and single pixel detector, can be advantageous in a range of application scenarios [1]. These include challenging wavelength ranges where focal plane array technologies are not available [2,3], terahertz frequencies [4–6], where precise timing and depth resolution are sought [7–13], or for multispectral [14–17], hyperspectral [18,19], and microscopy imaging [18,20,21], or imaging through scattering media [22,23]. Single pixel imaging has been developed over the last couple of decades since first reported by Duarte et al. [24]. The technique functions by creating the image structure through the insertion of patterned masks into imaging system (either between the light source and the target or between the target and the detector), with the light from the scene collected by a detector with only one pixel. The image is then reconstructed by associating a detected light level with the known pattern mask. The simplest pattern mask is the raster scan, where only one pixel in the mask is on at a time and this one pixel is scanned over the scene of interest with the single pixel detector recording the brightness at each position. Raster scanning is an inefficient use of the available light, scaling poorly with increasing resolution for pixel count and more efficient pattern sets have been developed [24–28].

#525753 https://doi.org/10.1364/OE.525753
Journal © 2024 Received 11 Apr 2024; revised 14 Jun 2024; accepted 14 Jun 2024; published 21 Jun 2024

Optics EXPRESS

In many applications, a fundamental barrier to practical adoption of the single pixel imaging technique is the relatively slow speed of applying the imaging masks compared to the potentially fast conventional imaging using a detector array. The fundamental limit to the speed of the imaging is defined by the frame rate of the device applying the pattern masks. The most common type of device used for the pattern masks is the Digital Multimirror Device (DMD). These arrays of a large number of micro-mirrors are able to produce a wide range of binary patterns that can be used as masks. However, DMDs are limited in their refresh frame rate to <30 kfps due to the mechanical nature of their pixel switching [1]. One technique often used to improve imaging speed is to reduce the number of image masks used, normally referred to as compressive sampling (CS) [24]. Reducing the number of masks results in an incomplete image, however, there can often be enough information to still create a useful image. There are numerous examples of DMDs being used, with or without CS, to achieve fast single pixel imaging at the maximum frame rate of the device [3,9,20,29–31]. Using CS is always a trade-off between the imaging frame rate and the resolution of the resulting images [32].

Instead of imaging speed being limited by DMDs, a few other techniques have been explored in order to increase the speed of single pixel imaging. LED arrays can enable a higher speed of pattern switching in illumination than is possible with a DMD, with a recent example showing exceptionally high speeds for a 32×32 array of LEDs as a light source and pattern mask [33,34]. The passive matrix addressed LED hardware is well suited to use of Hadamard pattern projection but presents challenges in scaling the array resolution and cannot operate with arbitrary pattern sets where individual pixel control is required. An alternative to a programmable device for illumination patterns is to use a technique from terahertz single pixel imaging [4,35] and use patterned masks mechanically scanned at high speed [36,37], where imaging up to 100 fps has been achieved. Instead of using etched patterns, Kilcullen et al. use laser scanning of a DMD surface to achieve 100 fps single pixel imaging [38]. Further examples of niche single pixel imaging at very high speeds include a technique that images a periodically repeating scene [39], use of frequency division multiplexing for high-speed microscopy [40]; and the high speed tracking of objects [41].

An important consideration with single pixel imaging is the choice of pattern masks. In Fig. 1, some of the pattern masks used here are shown displayed on the microLED array used in this work, where (a) shows the microLED array with every pixel switched on. It is possible, but time consuming, to use random binary patterns [10,42]. Imaging can be improved by ensuring 50% of pixels are on in a pattern [43], however, it is generally more efficient to use a known orthogonal pattern basis which can enable ideal reconstruction [44]. Examples of frequently chosen bases include ones derived from the Hadamard matrices [24] and Fourier transforms [15,25]. Both of these have the advantage of being well suited to CS for natural images as much of the information is usually within a small fraction of the possible spatial frequencies [44]. An example of a low spatial frequency Hadamard pattern is shown in Fig. 1(b). The noiselet pattern basis [28] can also achieve perfect reconstruction, but has similar characteristics to using random patterns. Different combinations of noiselet patterns form some given fraction of the pattern set on average leading to equal quality reconstructions regardless of specific pattern choice. Binary noiselet patterns are also easily generated, reducing pattern memory requirements, and have reduced coherence with common compression wavelet families, thereby theoretically requiring fewer measurements than Hadamard-based patterns to obtain a given reconstruction quality [28]. An example of a noiselet pattern is shown in Fig. 1(c). Instead of using a mathematically determined pattern basis, another route that has recently been explored is to use deep neural networks to reduce and optimise the pattern basis for a DMD to a fixed small number of patterns (333 and 666) to achieve video rate (30Hz and 15Hz) for general scenes [31].

In this paper we demonstrate the ways in which a recently developed microLED light projector [45] can display pattern masks at a high enough rate to enable very fast single pixel imaging and

Optics EXPRESS

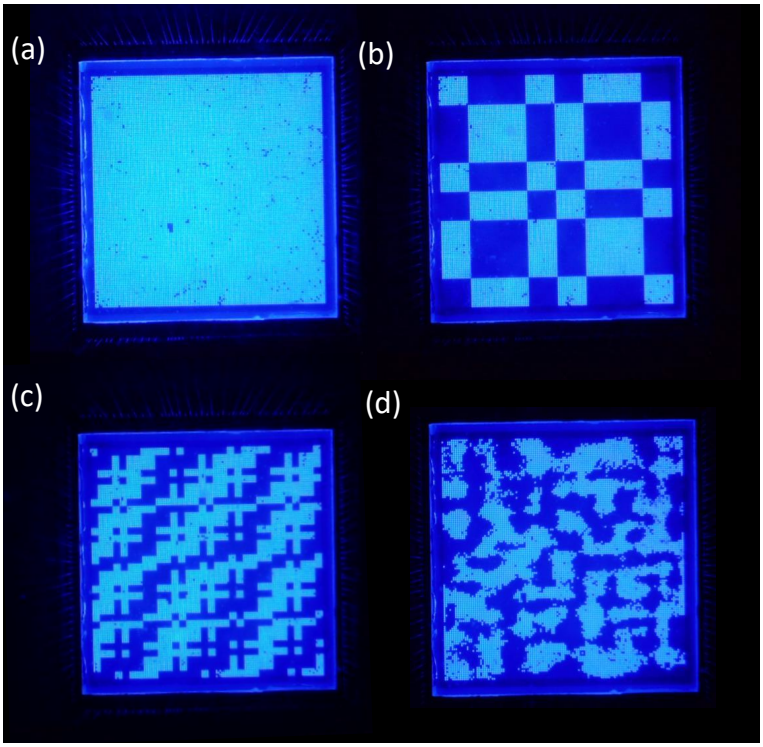

Fig. 1. Plan view optical microscope images of the microLED array, with array size 6×6 mm^2. (a) Shows the array with every pixel switched on, demonstrating the excellent uniformity and low number of dead pixels (<1%). The other images show the array displaying an example pattern from each of the three sets explored here (b) Hadamard, (c) noiselet and (d) deep-learned.

has the flexibility to switch between different pattern mask bases. By using a microLED array, we can display patterns an order of magnitude faster than most DMDs and with a maximum resolution here of 128×128 pixels can still perform single pixel imaging at a high resolution. We also make use of a deep learned pattern basis to demonstrate exceptionally fast single pixel imaging, with an imaging frame rate of 798 fps. The light projector is shown in Fig. 1(a), showing that the uniformity of pixel brightness is very good and the pixel yield is >99%.

2. Methods

Our microLED projector device is based on a 128×128 array of microLED pixels on a 50 μm pitch capable of displaying digital patterns at 500 kfps [45]. The light projector is fabricated from a c-plane GaN-on-sapphire wafer with a peak emission wavelength at 450 nm using standard LED fabrication. It is then flip-chip bonded onto a custom-designed CMOS driver chip using an indium based bonding process. The driver allows each pixel to be individually addressable, with a global shutter. This device is therefore a self-contained digital light projection system enabling a simpler, smaller and lower power light source for high speed single pixel imaging than comparable technologies such as DMDs. Full details and images of the system can be found in Ref. [45]. The microLEDs can be addressed at 399 kfps in the mode that is suitable for single pixel imaging, however, the current firmware implementation is implemented at 250 kfps to accommodate a number of complementary operation modes. Further development of the firmware will enable this system to run at higher frame rates.

Optics EXPRESS

Two optical arrangements are used to highlight different aspects of single pixel imaging with the microLED array. The first arrangement is shown in Fig. 2(a) and is a reflection geometry with the LED array imaged directly on to a target using a lens with focal length equal to 50 mm. In this work the target for the reflection setup was a Texas Instruments dlp7000 Digital Multimirror Device (DMD). The DMD could be set to display any binary image of interest and enabled better control of the scene being imaged. The scene shown in this work is a series of handwritten characters from the NIST special database 19 [46]. The light reflected from the DMD was collected by a single pixel detector with a condenser lens, focal length of 32 mm. The second arrangement, a simple transmission arrangement, is shown Fig. 2(b). The array is imaged onto a semi-transparent target using the same lens as in the reflection arrangement. The single pixel detector is then placed on the opposite side of the target with the same condenser lens as the reflection arrangement again used to focus the light on to the detector. For the work presented here, two different targets are shown, the 1951 USAF resolution test target and a 3D printed disk with holes in the shape of recognisable characters. The targets are shown in Visualization 1 and Visualization 2. In both setups the single pixel detector is an Onsemi Silicon Photomultiplier C-Series 10035. This detector was chosen as it provides very low background noise and is sensitive to small changes in light received from the target. In transmission measurements a neutral density filter had to be in front of the detector in order to prevent it saturating.

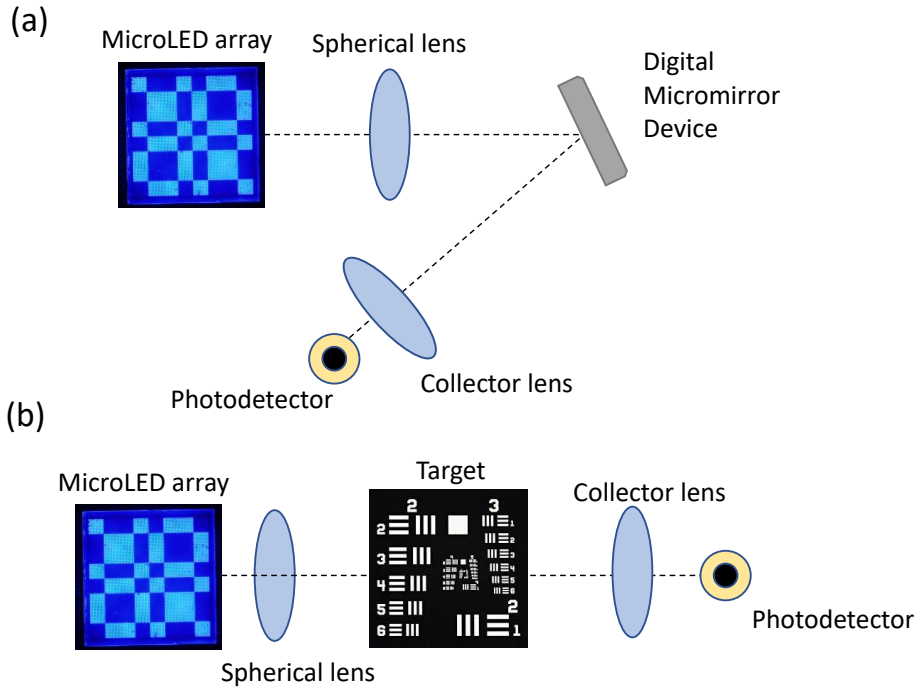

Fig. 2. Two different experimental setups were used in the single pixel imaging experiments discussed here. (a) Shows the reflection geometry that was used to image static scenes displayed on a Digital Micromirror Device (DMD) and (b) shows the transmission geometry where a semi-transparent target is imaged while placed between the light source and detector. This setup was used for imaging the USAF target and the spinning wheel in the video presented in Fig. 7. In both cases the microLED array is imaged onto the target with a spherical lens. The light from the target is collected and focused onto the single pixel detector.

Optics EXPRESS

Three different pattern sets have been tested with these setups, the Hadamard, Noiselet and Deep Learned pattern sets with an example pattern displayed on the microLED array shown for each in Fig. 1(b), (c) and (d) respectively. The methods for reconstructing the images are different for each these pattern sets and this will be outlined over the next few paragraphs.

Hadamard patterns. The Hadamard patterns are derived from the Hadamard matrices, which are square matrices with values 1 or −1 in each element. A matrix cannot be displayed in this form on a normal display and instead two patterns representing this matrix, one for the positive elements and one for the negative elements are displayed and the difference in detected light from those two displayed patterns is taken as the signal for the image reconstruction. The image I is calculated with [47],

$$I_{(x,y),M} = \frac{1}{M}\sum_{m=1}^{M} S_m P_{(x,y),m} \tag{1}$$

where $P_{(x,y),m}$ is the *mth* Hadamard pattern, S_m is the difference in detected signal between the two displayed patterns corresponding to that Hadamard pattern, with M total number of Hadamard patterns sampled. To perform CS, a fraction of the complete pattern set is used in the image reconstruction. In the case of the Hadamard patterns, the lower frequency patterns are selected as determined in the zigzag pattern described by Zhang et al. [44].

Noiselets. Noiselets are natively complex-valued, with −1, 0 and +1 magnitudes in both their real and imaginary parts, but Pastuszczak et al.'s transformations detailed in [28] allow a $m \times n$ noiselet sensing matrix to be replaced by a $(m + 1) \times n$ binary-valued matrix. The rows of this matrix are then reshaped into square patterns for display on the microLED array, with a difference coefficient S captured for each pattern and its inverse, as for the Hadamard experiment. A reverse transformation converts the measurements of S to complex-valued coefficients, which, together with the original $m \times n$ sensing matrix, are suitable input for standard CS reconstruction algorithms. We use Becker et al.'s efficient NESTA algorithm [48], enabling the total variation minimization option to bias reconstruction against high variance (i.e. noisy) solutions. CS with the Noiselet patterns can be performed by randomly choosing patterns to be included in the image.

Deep learning generated patterns. Deep learning algorithms can be used to generate a set of compressive sampling patterns for single pixel imaging that can more effectively sample the spatial frequency space than simple down-sampling of full pattern sets such as the Hadamard or Noiselet schemes. Deep learning [49] was used in a previous study [31] to optimise a binary {-1,1} pattern basis (coincidentally also of resolution 128 × 128) with a fixed number of patterns (333 and 666) that could be uploaded to a DMD (20 kHz) and applied in a single pixel camera setup to achieve video rate imaging (30 fps and 15 fps). The method [31] involved training a deep convolutional autoencoder neural network (DCAN) which simulated signal acquisition and reconstruction with the single pixel setup (DMD and single sensor). The objective of training a neural network is to find the weights or parameters associated with the network layers (encoding and decoding) which optimise performance. The desired number of encoding weights, in terms of desired resolution (128 × 128) and number of patterns (333 and 666) was hardcoded into the network architecture. Using this simulation approach, training was possible on large dataset of natural images [50] to obtain patterns for general scenes. Once trained, the optimised weights of the encoding layer became the pattern basis and were uploaded to the DMD for signal acquisition. The decoding layers were used to reconstruct the image from the signal.

In this work, the requirement for the number of patterns for the microLED light projector is 240, as each pattern must also have its inverse display and the FPGA memory is limited to 500 patterns (20 frames were also required for image separation). The number of encoding weights in the DCAN architecture [31] were set as 128 × 128 × 240. In this way, the modified DCAN simulates signal acquisition and reconstruction for the light projector. The model was retrained. All other details concerning the training were kept constant. Once retrained, the encoding weights

Optics EXPRESS

were uploaded to the light projector and the decoding layers were used to reconstruct the image from the signal as for the original single pixel setup. Mathematically, the signal is reconstructed using the decoding layers which can be thought of as a map $f : S - > I$ from signal space to image space. The map, f, is parameterised by the weights from the decoding layers, θ. $S \in Real^{240}$ and $I \in Real^{128x128}$.

Image reconstruction analysis. In order to evaluate the quality of the image reconstruction, a few metrics have been used to quantify the results. The structural similarity index measurement (SSIM) is a method that compares the similarity of two images, with a value of one indicating perfect similarity and a zero indicating no similarity. This is used to compare each image to a suitable reference image. Two reference images were used for each set of results. For each set the full 128×128 pixel image was used as the principal reference image, with the results quoted as SSIM(P). This image was chosen as it is the highest resolution image possible with each setup, regardless of the pattern set used. However, although of high resolution, this can also be the noisiest image in a given set, due to the high spatial frequency terms included in the image reconstruction. Therefore, in each set of results, the 128×128 pixel image was processed using the denoiseImage function in MATLAB (included in the deep learning toolbox) to obtain a reference image with suppression of high spatial frequency noise. Although better representing the ground truth of the scene, the denoised image may also incorporate unwanted artefacts from the processing. SSIM measurements using the denoised image as a reference are denoted as SSIM(D). The edge spread function is also calculated for some of the images. This function gives an indication of the blurriness of an image. It is performed by examining what should be a sharp edge in the reconstructed image and evaluates the spread of spatial frequencies. The calculated metric has a lower number for a sharper image.

3. Results

The results are presented in three sections, demonstrating different techniques of single pixel imaging with the microLED array. The first section shows the results of single pixel imaging with Hadamard and Noiselet patterns, in various resolutions. In the second section, CS is demonstrated with the Hadamard pattern set. In the deep learning section, the results of using a very low number of frames to reconstruct an image at the fastest rate possible with this microLED array are shown.

Uncompressed Imaging. Examples of the microLED array being used for single pixel imaging in a reflection set up are shown in Fig. 3 where the Hadamard pattern set has been used for the illumination of the scene and in Fig. 4 where the Noiselet patterns set has been used. In both cases the device is being operated at 250 kfps resulting in the imaging frame rate shown above image (a), (c) and (d). A 128×128 pixel image is shown in (a) of both figures, and the four displayed characters are clearly visible. Although this device shows excellent pixel uniformity, there will be some errors arising from the malfunctioning microLEDs (fewer than 160 pixels in this array). The only cluster of these malfunctioning LEDs can be observed in the reconstructed image near pixel (85, 85), corresponding to the upper bend in the letter *S*.

There has been no image processing applied after the image reconstruction for the Hadamard results in Fig. 3 and the resulting image shows visible noise. Some noise is expected in single pixel imaging due to the high spatial frequency patterns included in the summation and it is most likely being accentuated by the dead pixels on this prototype microLED array. A denoised version of this image, shown in (b), was generated using the denoiseImage function in MATLAB's deep learning toolbox. The denoised image shows a very close approximation of what was originally displayed on the DMD. Instead of using the light projector as a 128×128 pixel array, it can instead be used as a 64×64 or 32×32 pixel array, using macro-pixels consisting of 2×2 and 4×4 microLEDs respectively. These images are displayed in Fig. 3(c) and (d). The characters

Optics EXPRESS

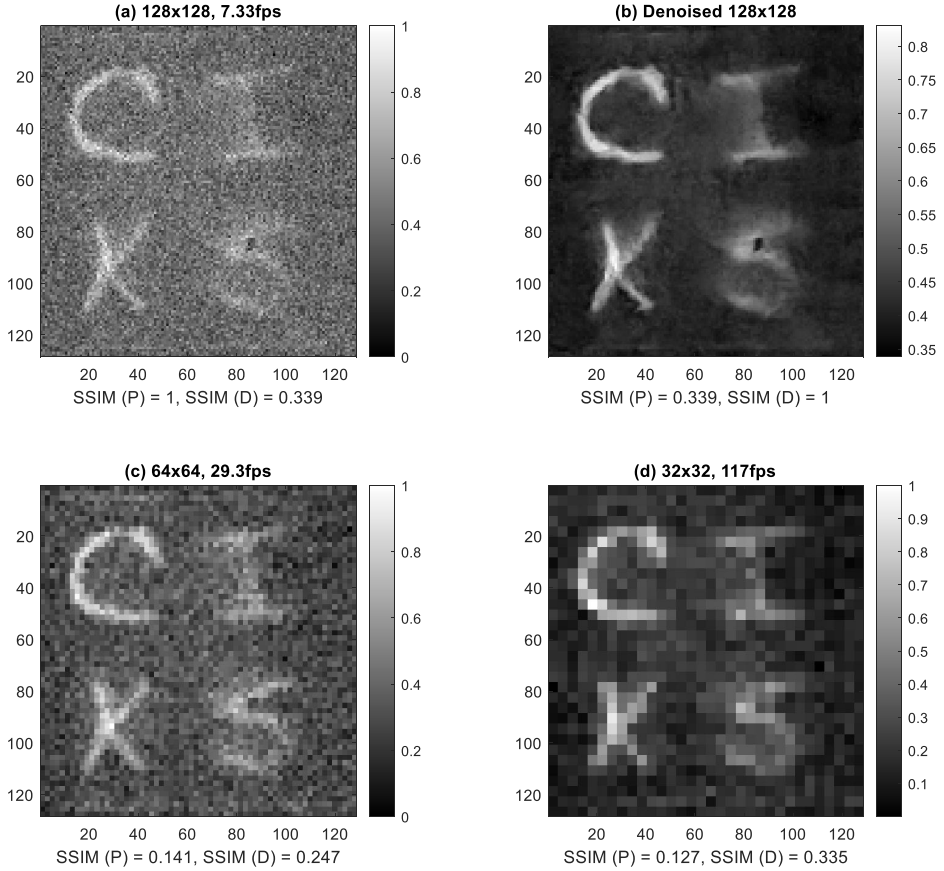

Fig. 3. Images of four characters displayed on a DMD, imaged in the reflection geometry using Hadamard patterns for illumination. The effective imaging frame rate is shown in the title and SSIM (P) is the comparison to image (a) and SSIM (D) is the comparison to image (b). (a) The 128×128 pixel image created using the full set of patterns for illumination, (b) the denoised version of (a), (c) uses the light projector as a 64×64 pixel array with (2×2 microLEDs used as macro pixels) and (d) a 32×32 pixel array with (4×4 microLEDs used as macro pixels). (c) and (d) therefore use reduced sets of Hadamard patterns corresponding to the number of macro pixels.

are still easily discerned, but with reduced resolution. The noise also improves, due to the highest spatial frequency Hadamard patterns no longer being included.

The Noiselet patterns in Fig. 4 shows images that are of a similar quality to the Hadamard patterns. This demonstrates the flexibility in imaging inherent with using a simple optical setup with a combined light source and pattern mask as either pattern set can be chosen without any change to the experimental procedure. The only change is loading a different pattern set onto the control FPGA.

Compressive Sampling. To explore compressive sampling, a transmission measurement was performed on a semi-transparent USAF resolution target (target shown in Visualization 1) using the Hadamard patterns, with the imaging results shown in Fig. 5. Figure 5(a-d) show the equivalent results for this target as were shown in the reflection setup in Fig. 3, demonstrating the reduced pixel imaging for this setup. The rest of the images, Fig. 5(e-h), show the CS results. The fraction is determined from the total number of frames taken for the full resolution 128×128

Optics EXPRESS

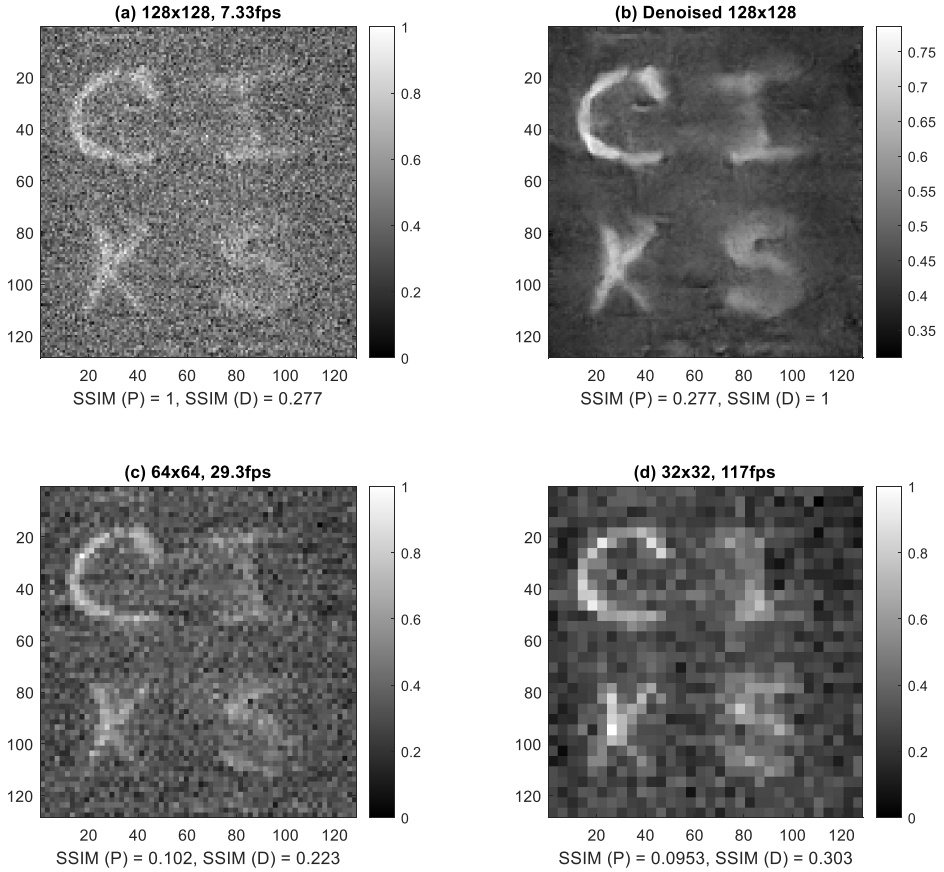

Fig. 4. Images of the four characters displayed on a DMD, imaged in the reflection geometry using Noiselet patterns for illumination. The effective imaging frame rate is shown in the title and SSIM (P) is the comparison to image (a) and SSIM (D) is the comparison to image (b). (a) The 128×128 pixel image created using the full set of patterns for illumination, (b) the denoised version of (a), (c) uses the light projector as a 64×64 pixel array with (2×2 microLEDs used as macro pixels) and (d) a 32×32 pixel array with (4×4 microLEDs used as macro pixels). (c) and (d) therefore use reduced sets of Noiselet patterns corresponding to the number of macro pixels.

pixel image shown in (a), with (e) showing $1/4$, (f) $1/8$, (g) $1/16$ and (h) $1/32$. Even in the case of only $1/32$ frames included, the image with the least number of frames in the reconstruction, the characters are still clearly legible with an imaging speed of 234 fps.

Deep Learned Pattern Set. The fastest imaging speed obtained in this work is performed using the deep learned pattern sets that were generated for this project. Image acquisition is performed with a pattern set consisting of only 500 patterns, 480 for the patterns as described in the methods section and 20 to enable separation of the images. This is equivalent to 3% of the total frames in the 128×128 pixel image in the Hadamard pattern results, shown in Fig. 5(a). First the USAF target was imaged with an identical arrangement to the Hadamard results, Fig. 6. High spatial frequency detail in the image is limited by the compact frame set, however, the outline of the USAF target is still clearly visible. This image was obtained with the microLED array at 250 kfps to enable direct comparison with earlier results.

Optics EXPRESS

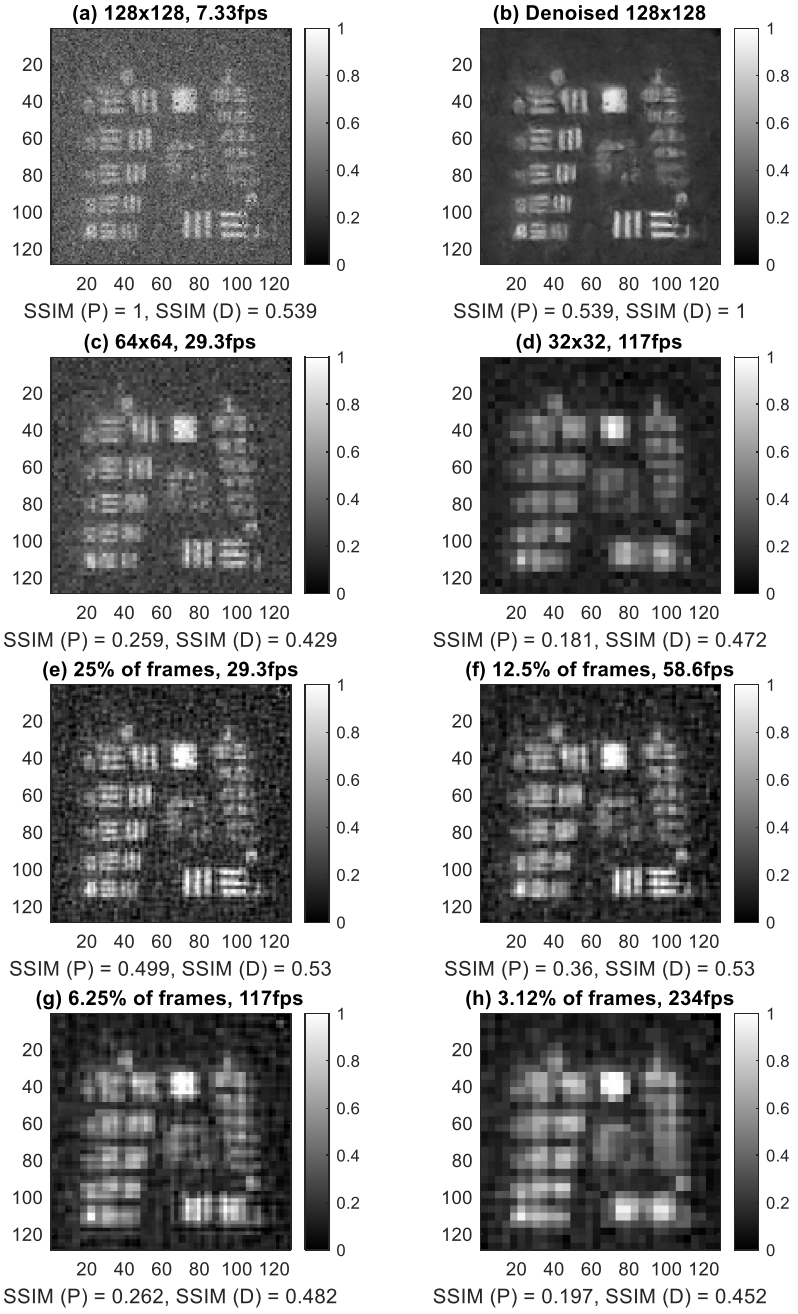

Fig. 5. Images of USAF resolution target (shown in Visualization 1), imaged in the transmission geometry using Hadamard patterns for illumination. The effective imaging frame rate is shown in the title and SSIM (P) is the comparison to image (a) and SSIM (D) is the comparison to image (b). (a) The 128×128 pixel image created using the full set of patterns for illumination, (b) the denoised version of (a), (c) uses the light projector as a 64×64 pixel array with (2×2 microLEDs used as macro pixels) and (d) a 32×32 pixel array with (4×4 microLEDs used as macro pixels). (c) and (d) therefore use reduced sets of Hadamard patterns corresponding to the number of macro pixels. Figures (e-h) show compressive sampling of the results for the full 128×128 pixel image, with (e) including $1/4$ of the frames from the full set, (f) $1/8$, (g) $1/16$ and (h) $1/32$ of the total frames included in that image.

Optics EXPRESS

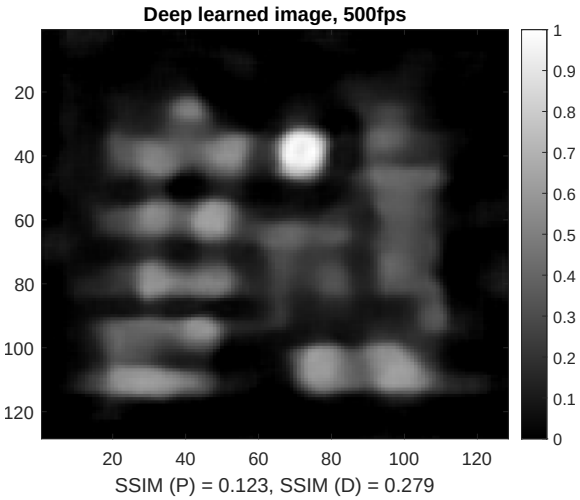

Fig. 6. The USAF target (shown in Visualization 1) imaged in a transmission setup with the deep learned pattern set. The values SSIM (P) and SSIM (D) compare the similarity of this result to the equivalent best Hadamard images, shown in Fig. 5(a) and (b) respectively. The imaging frame rate is 500 fps.

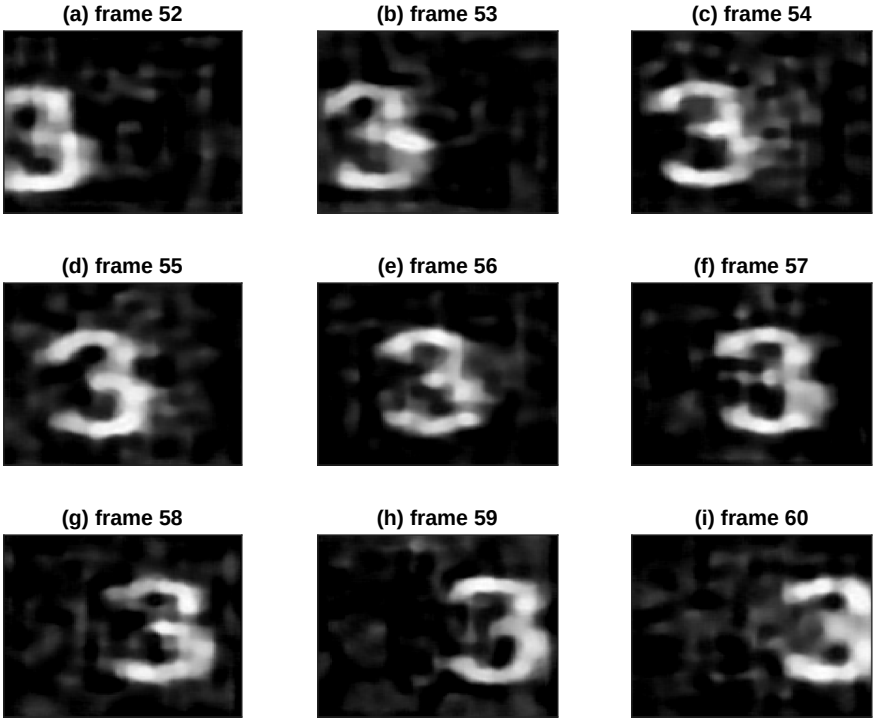

Fig. 7. Frames taken from a high-speed single pixel imaging video of characters on a spinning disk (shown in Visualization 2), showing a number three rotating through the frame. The disk was rotating at approximately 240 rpm, the microLED was displaying patterns at 399 kfps and the images are recorded at 798 fps. The numbers refer to the frame number in the full video, which can be viewed in Visualization 3.

Optics EXPRESS

As a demonstration of the highest possible frame rate of the microLED array, a video of a spinning disk was recorded with the array operating at 399 kfps (the disk is shown in Visualization 2). This results in real-time imaging performed at 798 fps. A rotating plastic disk with holes shaped as recognisable characters was 3D printed and attached to an optical chopper motor, which rotates the disk at approximately 240 rpm. The rotating disk is used as the target in a transmission arrangement and the results of imaging this disk are shown in Fig. 7, showing nine frames from a video of the disk rotating. The full video is available in Visualization 1. The still frames in the figure clearly show a number three rotating through the imaging frame.

4. Discussion

The results presented here across a number of different pattern sets demonstrate the flexibility of the microLED-on-CMOS projector as an emissive patterned light source for single pixel imaging. All of the various results are amongst the fastest imaging in the field, with regards to the different resolutions and degrees of CS. Table 1 summarises some of the imaging metrics used to compare the quality of single pixel imaging for the Hadamard patterns and the deep learned pattern set. The three metrics considered are the structural similarity index measurement (SSIM), the smallest resolvable feature on the resolution target and the edge spread function.

Table 1. Summary of the results of the single pixel imaging using Hadamard (Had) patterns and the deep learning patterns. The results all correspond to images shown in Figs. 5 and 6. The frame rates all correspond to the microLED array operating at 250 kfps. All of the resultant images are compared using SSIM to the 128 × 128 pixel image of that type (SSIM (P)), shown in Fig. 5(a) for Hadamard patterns and to the denoised version of the image (SSIM (D)) shown in Fig. 5(b). The smallest resolvable feature refers to the closest lines that are still resolvable in the imaging of the USAF target, the number corresponds to the number marked on the left part of the USAF target. A dash represents that none of the resolution features can be resolved. The edge spread function is measured at the top of the square feature near (80,30) in the images of the USAF target for each of the results.

Imaging setup	Frame rate (fps)	SSIM (P)	SSIM (D)	Resolvable feature	ESF
Had 128 × 128	7.33	1	0.539	2	4.61
Denoised 128 × 128	-	0.539	1	2	4.33
Had 64 × 64	29.3	0.259	0.429	3	5.09
Had 32 × 32	117	0.181	0.472	-	1.09
Had CS 25%	29.3	0.499	0.53	3	5.89
Had CS 12.5%	58.6	0.36	0.53	4	7.15
Had CS 6.25%	117	0.262	0.482	-	5.04
Had CS 3.13%	234	0.197	0.452	-	10.15
Deep-Learned	500	0.123	0.279	-	4.85

The number associated with the smallest resolvable feature corresponds to the label on the left side of the USAF target, most clearly seen in Fig. 5(a). A dash, representing no entry in the table, is given when none of the features on the left side could be resolved. A higher number here designates the resolution of a smaller object. The highest resolution features are observed in the slowest imaging methods, with faster imaging being unable to resolve smaller features, in line with expectations when performing single pixel imaging.

The edge spread function (ESF) is performed on the top edge of the square above the center of the USAF images, centered on pixel (80,30). The ESF is a metric that is related to the sharpness of intensity transitions in an image, with a lower number indicating a sharper edge. These results compare well to the SSIM results, showing the general trend that the more patterns used in the reconstruction, the better the ESF. There are exceptions to this trend as the lowest resolution

Optics EXPRESS

images show sharper edges due to their lack of information not due to an improvement in the faithful image capture and these therefore cannot be directly compared with the CS of higher resolution images 128×128 pixel image.

These metrics are all presented to show the full capabilities of imaging with this microLED array, the device can easily work with any pattern set and has significant flexibility in the speed vs imaging quality trade-off. This compares very well to other high-speed single pixel imaging arrangements where the experimental setup can make changing between different imaging modes difficult [34,36,39]. Here the pattern set is simply chosen and uploaded to the FPGA.

Comparing the 64×64 pixel image with the 25% CS image and the 32×32 pixel image with the 6.25% CS image illustrates a benefit of CS of a larger array being sub-sampled compared to the use of a smaller array size. In each of these cases the same number of patterns is used, but in the CS case we use a subset of the 128×128 pixel patterns and in the reduced case we are treating the array as lower resolution device by using macropixels consisting of 2×2 or 4×4 array pixels. The CS results outperform the reduced pixel according to the imaging metrics demonstrating the advantage of having 128×128 pixels compared to a smaller array, even when imaging at lower resolutions.

The deep learning pattern set was designed to demonstrate the fastest possible imaging with a 128×128 pixel array with only 500 frames available for the imaging (a limitation of the amount of memory in the FPGA controlling the microLED array in this measurement). This allowed the recording of very high-speed single pixel imaging. This is amongst the fastest demonstrations of high-speed single pixel imaging measurements to date, with the few faster examples showing limitations in the flexibility of the imaging or in the complexity of the imaging system. The imaging quality metrics do show a significant drop off in imaging with the deep learning compared to the Hadamard results, but this is expected with so few frames in the image. However, the deep learning pattern set was not optimised for this specific imaging configuration, as the model was trained on a data base of images of outdoor scenes. Further refinement of the model and training on images including digits and artificial test patterns (similar to those shown here), are expected to improve the imaging performance.

5. Conclusion

This work demonstrates the potential of high speed microLED light projectors in work requiring spatially structured light sources. This approach has a frame rate over an order of magnitude faster than the most widespread alternative technology, the digital micromirror display. Using one of these devices we have demonstrated high quality and high-speed single pixel imaging for a full 128×128 pixel image at 7.3 fps. By trading off image quality for imaging speed we achieve exceptionally fast single pixel imaging at almost 800 fps. The variety of pattern sets used shows the flexibility of imaging with this device compared to other techniques that can be more constrained to a particular pattern set. This work has demonstrated some of the more straightforward aspects of single pixel imaging and exploring imaging with more complex techniques, including ranging, or imaging in the ultraviolet is possible with this technology. MicroLED-on-CMOS arrays are compatible with industry standard micro-fabrication and packaging technologies, providing a route to future compact, power efficient chip systems. These devices can be fabricated with even larger numbers of pixels and higher data handling rates, using CMOS imaging array techniques, which will enable higher resolution and frame rate imaging than shown with the device available in this work.

Funding. Engineering and Physical Sciences Research Council (EP/M01326X/1, EP/S001751/1, EP/T00097X/1); Royal Academy of Engineering ("Research Chairs and Senior Research Fellowships").

Acknowledgments. We'd like to thank Sean Bommer for his assistance with preparing the spinning disk.

Disclosures. The authors declare no conflicts of interest.

Optics EXPRESS

Data availability. Data underlying the results presented in this paper are available in Ref. [51].

References

1. M. P. Edgar, G. M. Gibson, and M. J. Padgett, "Principles and prospects for single-pixel imaging," Nat. Photonics **13**(1), 13–20 (2019).
2. M.-J. Sun and J.-M. Zhang, "Single-Pixel Imaging and Its Application in Three-Dimensional Reconstruction: A Brief Review," Sensors **19**(3), 732 (2019).
3. M. P. Edgar, G. M. Gibson, R. W. Bowman, *et al.*, "Simultaneous real-time visible and infrared video with single-pixel detectors," Sci. Rep. **5**(1), 10669 (2015).
4. W. L. Chan, K. Charan, D. Takhar, *et al.*, "A single-pixel terahertz imaging system based on compressed sensing," Appl. Phys. Lett. **93**(12), 121105 (2008).
5. C. M. Watts, D. Shrekenhamer, J. Montoya, *et al.*, "Terahertz compressive imaging with metamaterial spatial light modulators," Nat. Photonics **8**(8), 605–609 (2014).
6. R. I. Stantchev, B. Sun, S. M. Hornett, *et al.*, "Noninvasive, near-field terahertz imaging of hidden objects using a single-pixel detector," Sci. Adv. **2**(6), e1600190 (2016).
7. W. Gong, C. Zhao, H. Yu, *et al.*, "Three-dimensional ghost imaging lidar via sparsity constraint," Sci. Rep. **6**(1), 26133 (2016).
8. M.-J. Sun, M. P. Edgar, G. M. Gibson, *et al.*, "Single-pixel three-dimensional imaging with time-based depth resolution," Nat. Commun. **7**(1), 12010 (2016).
9. Y. Zhang, M. P. Edgar, B. Sun, *et al.*, "3D single-pixel video," J. Opt. **18**(3), 035203 (2016).
10. B. Sun, M. P. Edgar, R. Bowman, *et al.*, "3D Computational Imaging with Single-Pixel Detectors," Science **340**(6134), 844–847 (2013).
11. G. A. Howland, P. B. Dixon, and J. C. Howell, "Photon-counting compressive sensing laser radar for 3D imaging," Appl. Opt. **50**(31), 5917–5920 (2011).
12. G. A. Howland, D. J. Lum, M. R. Ware, *et al.*, "Photon counting compressive depth mapping," Opt. Express **21**(20), 23822–23837 (2013).
13. Z. Zhang and J. Zhong, "Three-dimensional single-pixel imaging with far fewer measurements than effective image pixels," Opt. Lett. **41**(11), 2497–2500 (2016).
14. S. S. Welsh, M. P. Edgar, R. Bowman, *et al.*, "Fast full-color computational imaging with single-pixel detectors," Opt. Express **21**(20), 23068–23074 (2013).
15. L. Bian, J. Suo, G. Situ, *et al.*, "Multispectral imaging using a single bucket detector," Sci. Rep. **6**(1), 24752 (2016).
16. F. Rousset, N. Ducros, F. Peyrin, *et al.*, "Time-resolved multispectral imaging based on an adaptive single-pixel camera," Opt. Express **26**(8), 10550–10558 (2018).
17. Z. Zhang, S. Liu, J. Peng, *et al.*, "Simultaneous spatial, spectral, and 3D compressive imaging via efficient Fourier single-pixel measurements," Optica **5**(3), 315–319 (2018).
18. V. Studer, J. Bobin, M. Chahid, *et al.*, "Compressive fluorescence microscopy for biological and hyperspectral imaging," Proc. Natl. Acad. Sci. **109**(26), E1679–E1687 (2012).
19. J. Hahn, C. Debes, M. Leigsnering, *et al.*, "Compressive sensing and adaptive direct sampling in hyperspectral imaging," Digit. Signal Process. **26**, 113–126 (2014).
20. N. Radwell, K. J. Mitchell, G. M. Gibson, *et al.*, "Single-pixel infrared and visible microscope," Optica **1**(5), 285–289 (2014).
21. Y. Wu, P. Ye, I. O. Mirza, *et al.*, "Experimental demonstration of an Optical-Sectioning Compressive Sensing Microscope (CSM)," Opt. Express **18**(24), 24565–24578 (2010).
22. E. Tajahuerce, V. Durán, P. Clemente, *et al.*, "Image transmission through dynamic scattering media by single-pixel photodetection," Opt. Express **22**(14), 16945–16955 (2014).
23. V. Durán, F. Soldevila, E. Irles, *et al.*, "Compressive imaging in scattering media," Opt. Express **23**(11), 14424–14433 (2015).
24. M. F. Duarte, M. A. Davenport, D. Takhar, *et al.*, "Single-pixel imaging via compressive sampling," IEEE Signal Process. Mag. **25**(2), 83–91 (2008).
25. Z. Zhang, X. Ma, and J. Zhong, "Single-pixel imaging by means of Fourier spectrum acquisition," Nat. Commun. **6**(1), 6225 (2015).
26. B.-L. Liu, Z.-H. Yang, X. Liu, *et al.*, "Coloured computational imaging with single-pixel detectors based on a 2D discrete cosine transform," J. Mod. Opt. **64**(3), 259–264 (2017).
27. M. Alemohammad, J. R. Stroud, B. T. Bosworth, *et al.*, "High-speed all-optical Haar wavelet transform for real-time image compression," Opt. Express **25**(9), 9802–9811 (2017).
28. A. Pastuszczak, B. Szczygiel, M. Mikolajczyk, *et al.*, "Efficient adaptation of complex-valued noiselet sensing matrices for compressed single-pixel imaging," Appl. Opt. **55**(19), 5141–5148 (2016).
29. J. Zheng and E. L. Jacobs, "Video compressive sensing using spatial domain sparsity," Opt. Eng. **48**(8), 087006 (2009).
30. Z. Zhang, X. Wang, G. Zheng, *et al.*, "Fast Fourier single-pixel imaging via binary illumination," Sci. Rep. **7**(1), 12029 (2017).
31. C. F. Higham, R. Murray-Smith, M. J. Padgett, *et al.*, "Deep learning for real-time single-pixel video," Sci. Rep. **8**(1), 2369 (2018).

Optics EXPRESS

32. X. Zhu, Y. Li, Z. Zhang, *et al.*, "Adaptive real-time single-pixel imaging," Opt. Lett. **49**(4), 1065–1068 (2024).
33. Z.-H. Xu, W. Chen, J. Penuelas, *et al.*, "1000 fps computational ghost imaging using LED-based structured illumination," Opt. Express **26**(3), 2427–2434 (2018).
34. H. Huang, L. Li, Y. Ma, *et al.*, "25,000 fps Computational Ghost Imaging with Ultrafast Structured Illumination," Electron. Mater. **3**(1), 93–100 (2022).
35. H. Shen, L. Gan, N. Newman, *et al.*, "Spinning disk for compressive imaging," Opt. Lett. **37**(1), 46–48 (2012).
36. E. Hahamovich, S. Monin, Y. Hazan, *et al.*, "Single pixel imaging at megahertz switching rates via cyclic Hadamard masks," Nat. Commun. **12**(1), 4516 (2021).
37. W. Jiang, J. Jiao, Y. Guo, *et al.*, "Single-pixel camera based on a spinning mask," Opt. Lett. **46**(19), 4859–4862 (2021).
38. P. Kilcullen, T. Ozaki, and J. Liang, "Compressed ultrahigh-speed single-pixel imaging by swept aggregate patterns," Nat. Commun. **13**(1), 7879 (2022).
39. W. Jiang, Y. Yin, J. Jiao, *et al.*, "2,000,000 fps 2D and 3D imaging of periodic or reproducible scenes with single-pixel detectors," Photonics Res. **10**(9), 2157–2164 (2022).
40. H. Kanno, H. Mikami, and K. Goda, "High-speed single-pixel imaging by frequency-time-division multiplexing," Opt. Lett. **45**(8), 2339–2342 (2020).
41. S. Li, Y. Cai, Y. Wang, *et al.*, "Single-pixel imaging of a translational object," Opt. Express **31**(4), 5547–5560 (2023).
42. J. H. Shapiro, "Computational ghost imaging," Phys. Rev. A **78**(6), 061802 (2008).
43. F. Ferri, D. Magatti, L. A. Lugiato, *et al.*, "Differential Ghost Imaging," Phys. Rev. Lett. **104**(25), 253603 (2010).
44. Z. Zhang, X. Wang, G. Zheng, *et al.*, "Hadamard single-pixel imaging versus Fourier single-pixel imaging," Opt. Express **25**(16), 19619–19639 (2017).
45. N. B. Hassan, F. Dehkhoda, E. Xie, *et al.*, "Ultrahigh frame rate digital light projector using chip-scale LED-on-CMOS technology," Photonics Res. **10**(10), 2434–2446 (2022).
46. "NIST Special Database 19," NIST (2010). Last Modified: 2019-04-27T09:36-04:00.
47. G. M. Gibson, S. D. Johnson, and M. J. Padgett, "Single-pixel imaging 12 years on: a review," Opt. Express **28**(19), 28190–28208 (2020).
48. S. Becker, J. Bobin, and E. J. Candès, "NESTA: A Fast and Accurate First-Order Method for Sparse Recovery," SIAM J. on Imaging Sci. **4**(1), 1–39 (2011).
49. I. J. Goodfellow, Y. Bengio, and A. Courville, *Deep Learning* (MIT Press, 2016).
50. A. Coates, A. Ng, and H. Lee, "An Analysis of Single-Layer Networks in Unsupervised Feature Learning," in *Proceedings of the Fourteenth International Conference on Artificial Intelligence and Statistics*, (JMLR Workshop and Conference Proceedings, 2011), pp. 215–223. ISSN: 1938–7228.
51. G. Johnstone, "Data for: "High Speed Single Pixel Imaging using a MicroLED-on-CMOS Light Projector"" University of Strathclyde (2024), https://doi.org/10.15129/34945828-c43d-43d1-b6f8-cba1036d379e.